



Radiation balance in a cloudy atmosphere with account for the 3D effects

L.P. Bass^a, O.V. Nikolaeva^a, V.S. Kuznetsov^b, A.A. Kokhanovsky^{c,*}

^a Keldysh Institute of Applied Mathematics, Moscow, Russia

^b Research Scientific Center "Kurchatov Institute", Moscow, Russia

^c Institute of Remote Sensing, Bremen University, Germany

ARTICLE INFO

Article history:

Received 17 July 2009

Received in revised form 28 October 2009

Accepted 3 December 2009

Keywords:

Radiative transfer

Clouds

3D effects

ABSTRACT

In this paper we derive radiation balance equations for the cloudy atmosphere with account for horizontal inhomogeneity effects. It is assumed that the clear sky and cloud occupy two different half-spaces separated by a vertical plane. Numerical results for corresponding fluxes are derived using the 3D code RADUGA based upon the discrete ordinate method. It is shown how "jump" of optical properties forms shadowing or brightening at both the cloud edge and the neighboring clear sky.

© 2009 Elsevier B.V. All rights reserved.

1. Introduction

The spatial distribution of brightness of broken cloud fields is very inhomogeneous both for reflected and transmitted solar light (Marshak et al., 2000; Varnai and Marshak, 2002). Clearly, this is the case for the absorptance as well. A humid aerosol layer surrounding the cloud could be a factor (Redemann et al., 2009). However, the careful analysis of the problem indicates that the 3D radiative interaction between clouds and surrounding clear areas is a major factor explaining corresponding extrema (Varnai and Marshak, 2009). Studies of solar light propagation based on the discrete ordinate method (Bass et al., 1986) (code RADUGA) in 2D regions, containing both cloud and clear sky (aerosol) with one vertical common boundary, shows (Nikolaeva et al., 2005) that brightness extrema in the vicinity of a cloud edge occur even if an intermediate aerosol layer is absent.

The origin of extrema of the intensity of solar light reflected and transmitted by the cloudy atmosphere is studied in this paper. Only one factor, namely, the horizontal

variations of optical properties of the atmosphere is taken into account. To eliminate the influence of intermediate layers, we consider a model problem, where a cloud and an aerosol (clear sky) have only one common (vertical) boundary $x = 0$ (see Fig. 1). Besides, both media are assumed to be homogeneous. Hence, the 3D radiative effects occur only in the vicinity of the cloud edge. Also it is clear that far from the common boundary both reflected and transmitted light intensities depend only on the height z .

We simulate the radiative transfer in atmosphere using the 3D transport equation and the discrete ordinate method (Section 2). Applying the radiative balance relation for the whole spatial region, not for a single pixel, see Section 3, it is shown how the horizontal radiative transfer caused by a "jump" of optical properties of a medium under consideration forms shadowing or brightening at both cloud edge and neighboring clear sky (Section 4).

2. Mathematical model

Let us put the coordinate origin at the top of the atmosphere and direct the axis z to the ground. We place the axis y along the boundary of the cloud and aerosol (in the horizontal direction, see Fig. 1). It is assumed that the illumination direction is perpendicular to the axis y (the azimuth ϕ of the

* Corresponding author.

E-mail address: alexk@iup.physik.uni-bremen.de (A.A. Kokhanovsky).

3. Radiation balance

We derive the balance equation for the whole region, rather than just for one pixel (Titov, 1998; Widlowski et al., 2006). Let introduce functions, defining radiation fluxes at the vertical boundaries of the cross section $[-X_L, X_R] \times [0, Z]$ of unit width:

$$j_R(z) = \int_0^\pi d\theta \sin\theta \int_0^{2\pi} d\varphi \sin\theta \cos\varphi I(X_R, z, \theta, \varphi) \quad (10a)$$

–at the right boundary $x = X_R$,

$$j_L(z) = - \int_0^\pi d\theta \sin\theta \int_0^{2\pi} d\varphi \sin\theta \cos\varphi I(-X_L, z, \theta, \varphi) \quad (10b)$$

–at the left boundary $x = -X_L$.

Each of these functions is positive if the main radiation flux across corresponding spatial point of a boundary is directed out of the cross section and negative in the opposite case.

We introduce fluxes of radiation leaving the cross section via its top and bottom boundaries

$$j_T(x) = \int_{\cos\theta < 0} d\theta \sin\theta |\cos\theta| \int_0^{2\pi} d\varphi I(x, 0, \theta, \varphi) \quad (11a)$$

–for the top boundary,

$$j_B(x) = \int_{\cos\theta > 0} d\theta \sin\theta \cos\theta \int_0^{2\pi} d\varphi I(x, Z, \theta, \varphi) \quad (11b)$$

–for the bottom boundary.

The absorptivity c at a given point $M(x, z)$ can be found using the following equation:

$$c(x, z) = \sigma_{abs}(x, z) \Phi(x, z), \quad (12)$$

where $\sigma_{abs} = (1 - \omega_0) \sigma_{ext}$ is the absorption coefficient and

$$\Phi(x, z) = \int_0^\pi d\varphi \int_0^\pi d\theta \sin\theta I(x, z, \theta, \varphi) \quad (13)$$

is the actinic flux.

To obtain the radiative balance relation we integrate the Eq. (1) over angles θ and φ and the spatial variables x, z in the cross section $[-X_L, X_R] \times [0, Z]$ of unit width, see Fig. 1, taking into account the normalization equality (3) and boundary conditions (4)–(6). In particular, the integration of the first term on the left side leads to the expression

$$\begin{aligned} & \int_0^Z dz \int_{-X_L}^{X_R} dx \int_0^\pi d\theta \sin\theta \int_0^{2\pi} d\varphi \sin\theta \cos\varphi \frac{\partial I}{\partial x} \quad (14) \\ &= \int_0^Z dz \int_0^\pi d\theta \sin\theta \int_0^{2\pi} d\varphi \sin\theta \cos\varphi [I(X_R, z, \theta, \varphi) - I(-X_L, z, \theta, \varphi)] \\ &= \int_0^Z dz \{j_R(z) + j_L(z)\} \end{aligned}$$

It follows for the second term

$$\begin{aligned} & \int_0^Z dz \int_{-X_L}^{X_R} dx \int_0^\pi d\theta \sin\theta \int_0^{2\pi} d\varphi \cos\theta \frac{\partial I}{\partial z} \quad (15) \\ &= \int_{-X_L}^{X_R} dx \int_0^\pi d\theta \sin\theta \int_0^{2\pi} d\varphi \cos\theta [I(x, Z, \theta, \varphi) - I(x, 0, \theta, \varphi)] \\ &= \int_{-X_L}^{X_R} dx \left[- \int_{\cos\theta > 0} d\theta \sin\theta \cos\theta \int_0^{2\pi} d\varphi I(x, 0, \theta, \varphi) \right. \\ & \quad + \int_{\cos\theta > 0} d\theta \sin\theta \cos\theta \int_0^{2\pi} d\varphi I(x, Z, \theta, \varphi) \\ & \quad \left. + \int_{\cos\theta < 0} d\theta \sin\theta |\cos\theta| \int_0^{2\pi} d\varphi I(x, 0, \theta, \varphi) \right] \\ &= \int_{-X_L}^{X_R} dx \{-F_0 \cos\theta + j_B(x) + j_T(x)\}. \end{aligned}$$

One finds the difference of the last term at the left side and the scattering integral

$$\begin{aligned} & \int_0^Z dz \int_{-X_L}^{X_R} dx \int_0^\pi d\theta \sin\theta \int_0^{2\pi} d\varphi \left[\sigma_{ext} I - \frac{\sigma_{sca}}{4\pi} \int_0^\pi d\theta' \sin\theta' \int_0^{2\pi} d\varphi' I(x, z, \theta', \varphi') p(x, z, \chi) \right] \\ &= \int_0^Z dz \int_{-X_L}^{X_R} dx \int_0^\pi d\theta \sin\theta \int_0^{2\pi} d\varphi I(x, z, \theta, \varphi) \left[\sigma_{ext} - \frac{\sigma_{sca}}{4\pi} \int_0^\pi d\theta' \sin\theta' \int_0^{2\pi} d\varphi' p(x, z, \chi) \right] \\ &= \int_0^Z dz \int_{-X_L}^{X_R} dx c(x, z) \quad (16) \end{aligned}$$

The transformation of the first line in this equality to the second one is carried out via variable changes; the transformation of the second line to the third one is based upon the normalization condition (3).

Combining the equalities (14)–(16), one obtains the required balance relation

$$\begin{aligned} & \int_0^Z dz \{j_R(z) + j_L(z)\} + \int_{-X_L}^{X_R} dx \{j_B(x) + j_T(x)\} + \int_0^Z dz \int_{-X_L}^{X_R} dx c(x, z) \\ &= (X_L + X_R) F_0 \cos\theta, \quad (17) \end{aligned}$$

having obvious physical sense. The term $(X_L + X_R) F_0 \cos\theta$ at the right side defines the full energy of radiation, entering the cross section across its top boundary. The first integral at the left side is equal to the difference of energy of radiation leaving the cross section and entering it across vertical boundaries $x = X_R$ and $x = -X_L$. The second integral is equal to energy of radiation leaving the region via the bottom boundary $z = Z$ and the top $z = 0$. The double integral at the left side defines energy absorbed within the cross section. Eq. (17) is a major result of this work.

Let us assume now that the cross section is infinite and homogeneous over x ; such a model corresponds to a light scattering plane-parallel layer of height Z . Then intensity does not depend on x and the balance relation (17) has a form (as $-X_L \rightarrow -\infty, X_R \rightarrow \infty$)

$$j_B + j_T + \int_0^Z dz c(z) = F_0 \cos\theta, \quad (18)$$

where

$F_0 \cos\Theta$	energy of radiation, entering the layer across an unit area of its top boundary,
j_T	energy of radiation, reflected by an unit area of the top boundary,
j_B	energy of radiation, transmitted by an unit area of the bottom boundary,
$\int_0^z dz c(z)$	energy of radiation absorbed in the layer.

Let us introduce the reflectance and transmittance for the slab layer

$$R = \frac{j_T}{F_0 \cos\Theta}, \quad T = \frac{j_B}{F_0 \cos\Theta}. \quad (19)$$

Then the radiative balance relation (18) can be written as

$$R + T + A = 1, \quad (20)$$

where

$$A = k \int_0^z dz \sigma_{abs}(z) \Phi(z) \quad (21)$$

is the absorptance and $k = 1/F_0 \cos\Theta$. Usually, the absorptance is found as a difference $1 - R - T$ from calculated values of the reflectance and transmittance. However, it can result in errors as $A \rightarrow 0$. Therefore, calculations using Eq. (21) are more accurate. It follows for a vertically homogeneous layer from Eq. (21):

$$A = k \langle \Phi \rangle \tau_{abs} \quad (22)$$

or alternatively

$$A = k \Phi(z_0) \tau_{abs}, \quad (23)$$

where

$$\tau_{abs} = \sigma_{abs} Z, \quad \langle \Phi \rangle = \frac{1}{Z} \int_0^z \Phi(z) dz \approx \Phi(z_0) \quad (24)$$

and we used the theorem on average. It follows from these equations that the average actinic flux in the scattering layer can be calculated as

$$\langle \Phi \rangle = \frac{1 - R - T}{k \tau_{abs}}. \quad (25)$$

The actinic flux is a very important parameter for atmospheric chemistry studies because it determines the photolysis rate, which is influenced by 3D effects as well. The same applies to the heating rate and the spectral density of radiation $u = \Phi/c_0$, where c_0 is the speed of light.

4. Numerical results

In this section we present numerical results for the spatial distribution of radiation absorbed, reflected and transmitted

by a clear sky–cloud system. The following parameters are assumed in calculations:

- Zenith angle of the sun Θ : 60° .
- Azimuth Φ : $0^\circ, 180^\circ$.
- Height of the system: $Z = 4$ km.
- Width of the system: $X_L = 60$ km, $X_R = 30$ km.
- Extinction coefficient of a clear sky region (no absorption assumed): $\sigma_{ext}^{aer} = 0.125 \text{ km}^{-1}$.
- Extinction coefficient in a cloud $\sigma_{ext}^{aer} = 2.5 \text{ km}^{-1}$.
- Single scattering albedo in a cloud ω_0^{cloud} : 0.9, 0.95, 0.99, 1.0.
- The bottom boundary is black.

Both cloud and aerosol are assumed to be horizontally homogeneous media. Aerosol scattering is simulated using the Henyey–Greenstein phase function with the asymmetry parameter $g = 0.7$, being decomposed into P_{23} Legendre series. Cloud C1 phase function is obtained via Mie theory for the wavelength 412 nm (van de Hulst, 1980). Its peak is replaced by delta-function using the delta-M method (Wiscombe, 1977), and the remaining regular component is presented by P_{27} Legendre series.

The solution of the problem under consideration (the light field intensity $I(x, z, \theta, \varphi)$) is found via the discrete ordinate method using the code RADUGA (Nikolaeva et al., 2005) assuming the underlying black surface. This code is based upon mesh schemes of the discrete ordinate method, when regular meshes over spatial and angular variables are introduced and the transport equation in each mesh is approximated by algebraic relations. They are the balance equalities, that resulted from the integration of the radiative transfer equation over a mesh (not whole region), and the piece-linear approximation to a solution desired in a mesh. Next the successive-orders-of-scattering (SOS) iteration process with the diffusion-synthetic acceleration (DSA) method (Marchuk and Lebedev, 1986; Larsen, 1982), where acceleration correction to a solution after each SOS iteration is found as the diffusion equation solution, are used to resolve this algebraic system. Note that the adaptive irregular spatial meshes, the ray tracing method to construct mesh approximation and the SOS iteration method with interpolation acceleration technique to resolve an approximate system are employed in the SHDOM code (Evans, 1998).

We show the numerical results for the following functions (see Figs. 2–6):

1. $J_R(z) = \frac{j_R(z)}{F_0 \cos\Theta}$, $J_L(z) = \frac{j_L(z)}{F_0 \cos\Theta}$ – normalized horizontal fluxes,
2. $R(x) = \frac{j_T(x)}{F_0 \cos\Theta}$, $T(x) = \frac{j_B(x)}{F_0 \cos\Theta}$ – reflectance and transmittance,
3. $C(x, z) = \frac{c(x, z)}{F_0 \cos\Theta}$ – absorptance,
4. $\varepsilon_R(x) = 1 - R(x) / R^{\text{IPA}}(x)$, $\varepsilon_T(x) = 1 - T(x) / T^{\text{IPA}}(x)$,

(26)

where $R^{\text{IPA}}(x)$ and $T^{\text{IPA}}(x)$ are obtained via the independent pixel approximation (IPA) method.

The illumination directions are depicted in all figures by arrows. The illumination from a clear sky side corresponds to the azimuth $\Phi = 0^\circ$. The azimuth 180° is for the illumination from a cloud side.

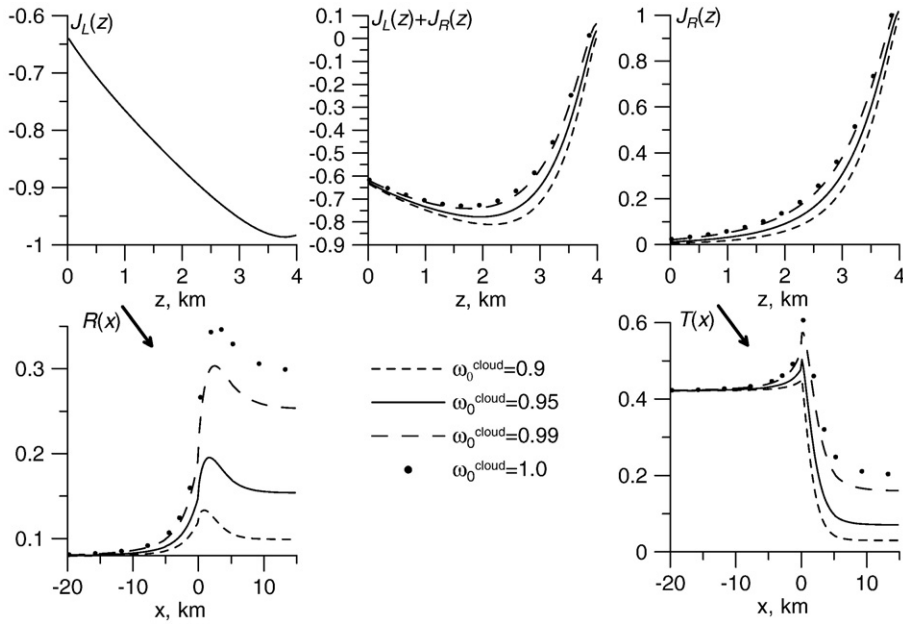


Fig. 2. The normalized horizontal fluxes $J_R(z)$, $J_L(z)$, their sum $J_L(z) + J_R(z)$, transmittance $T(x)$ and reflectance $R(x)$ for illumination from the clear sky side ($\phi = 0^\circ$).

Functions $\varepsilon_R(x)$ and $\varepsilon_T(x)$ are not close to zero only in the vicinity of the boundary separating clear sky and a cloud. They have jumps in vicinity of the media boundary by definition (26) due to the fact that IPA coefficients R^{IPA} and T^{IPA} are very different for a cloud (for $x = 0^+$) and a clear sky (for $x = 0^-$), whereas 2D coefficients $R(x)$ and $T(x)$ are smooth functions.

The dimensions of regions, where 3D effects are of importance (x_r^{aer} , x_t^{aer} , x_r^{cloud} , and x_t^{cloud}) can be found from the following equations

$$\max_{x < -x_t^{aer}} |\varepsilon_R(x)| = 0.05, \quad \max_{x < -x_t^{aer}} |\varepsilon_T(x)| = 0.05 \text{—in an aerosol} \quad (27a)$$

$$\max_{x > x_r^{cloud}} |\varepsilon_R(x)| = 0.05, \quad \max_{x > x_r^{cloud}} |\varepsilon_T(x)| = 0.05 \text{—in a cloud.} \quad (27b)$$

They are presented in Tables 1 and 2.

In the case $\theta = 60^\circ$, $\phi = 0^\circ$, and $\omega_0^{cloud} = 1$ (the illumination from a clear sky side, see Figs. 2 and 3), the flux $J_R(z)$ is positive, the flux $J_L(z)$ is negative, and the sum of these fluxes $J_L(z) + J_R(z)$ is negative almost everywhere. So the most radiation moves from a clear sky to a cloud (in the direction of the direct light) via the vertical boundaries of the cross section, but more radiation enters the region than leaves it. “Superfluous” radiation leaves the cross section near the vertical boundary forming maxima in transmittance $T(x)$ and reflectance $R(x)$ (brightening effect).

Let us consider now the case at $\Phi = 180^\circ$ (illumination from a cloud side, see Figs. 4 and 5). The flux $J_R(z)$ is negative, the flux $J_L(z)$ is positive, the sum of these fluxes $J_L(z) + J_R(z)$ is positive almost everywhere. So the most photons move from a cloud to a clear sky region (in the direction of direct light) via the vertical boundaries of the cross section, but more radiation leaves the region rather than enters it. This produces minima of transmittance $T(x)$ and reflectance $R(x)$ near the vertical boundary (shadowing effect).

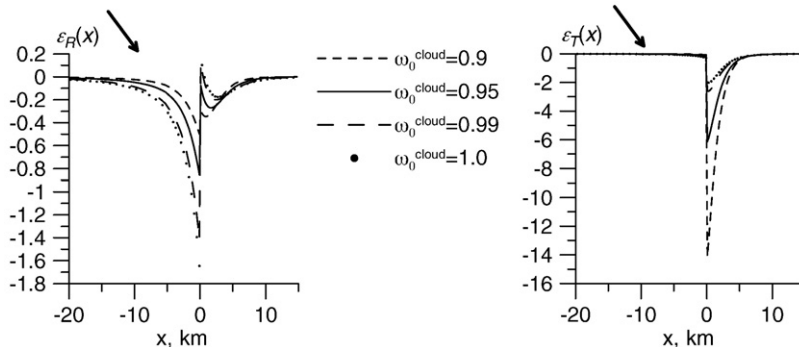


Fig. 3. Functions $\varepsilon_R(x)$ and $\varepsilon_T(x)$ for illumination from the clear sky side ($\phi = 0^\circ$).

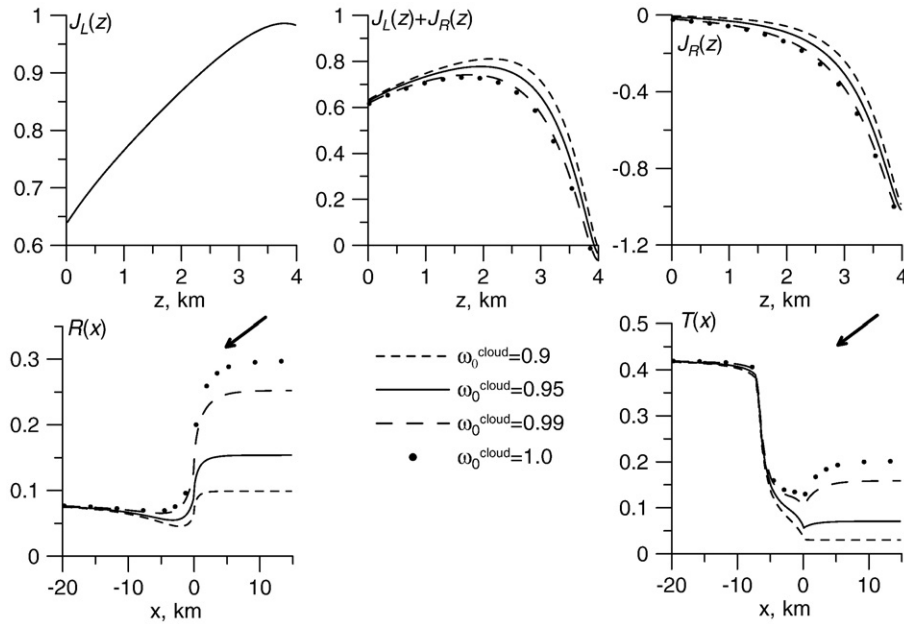


Fig. 4. The normalized horizontal fluxes $J_R(z)$ and $J_L(z)$, their sum $J_L(z) + J_R(z)$, transmittance $T(x)$ and reflectance $R(x)$ for illumination from the cloudy portion of the sky ($\phi = 180^\circ$).

Note, if both zones were identical, sum $J_L(z) + J_R(z)$ should be equal to zero and transmittance $T(x)$ and reflectance $R(x)$ should be constant functions of x (no brightening and shadowing effects).

If single scattering albedo $\omega_0^{\text{cloud}} < 1$, some radiation is absorbed in a cloud. This process leads to the decrease of the reflectance and transmittance in the aerosol boundary layer, but does not change these parameters of light field far away from the boundary of the medium, as one might expect. We found that the decrease of the cloud single scattering albedo leads to the reduction of the brightening effect in a clear sky portion of the scene. The shadowing effect is enhanced then. This leads to the decrease/increase of the sizes of boundary layers defined above (in a clear sky) if ω_0^{cloud} decreases (see Tables 1 and 2).

The decrease of single scattering albedo ω_0^{cloud} is the reason why the reflectance $R(x)$ and the transmittance $T(x)$ decrease at all points at the top and bottom boundaries of a cloud, correspondingly (far away from the interior boundary and in its vicinity). Then the cloud boundary layers decrease too.

The absorptance $C(x, z)$ for two cases of illumination ($\phi = 0^\circ$ and $\phi = 180^\circ$) is presented in Fig. 6. It can be seen the greatest absorption, and, therefore, the actinic flux and the photolysis rate, takes place near planes, across which the direct light from the sun enters a cloud. They are the top boundary (for both cases) and the left boundary (for illumination from a clear sky side). The smallest absorption takes place near the bottom cloud boundary, where the light intensity is the smallest. It follows that $C(x, z)$ does not depend on x in deep layers of a cloud far away from the boundaries. We conclude that broken cloud fields significantly modify the radiative fluxes, the actinic flux and the photolysis rates at the regions close to the cloud boundaries.

5. Conclusion

The technique to study the radiation intensity distribution in the horizontally inhomogeneous clear sky–cloud system is presented. The technique is applied to a model problem, in which each medium (both an aerosol and a cloud) is homo-

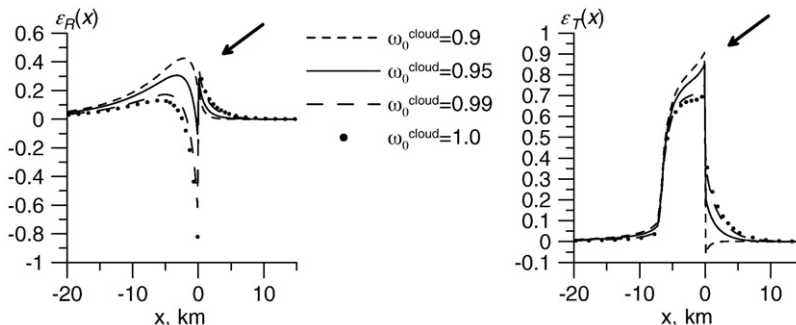


Fig. 5. Functions $\epsilon_R(x)$ and $\epsilon_T(x)$ for illumination from the cloudy portion of the sky ($\phi = 180^\circ$).

Table 1

Sizes of boundary layers x_r^{aer} and x_r^{cloud} (km), where 3D effects exist, for reflectance $R(x)$ at various values of the single scattering albedo ω_0^{cloud} and the solar azimuth ϕ . The solar zenith angle is equal to 60° .

ω_0^{cloud}	$\phi = 180^\circ$		$\phi = 0^\circ$	
	x_r^{aer}	x_r^{cloud}	x_r^{aer}	x_r^{cloud}
0.9	20.25	0.90	6.25	5.25
0.95	18.75	1.70	9.25	6.25
0.99	16.75	3.30	13.25	7.25
1.0	15.25	3.90	14.25	7.75

Table 2

Sizes of boundary layers x_r^{aer} and x_r^{cloud} (km), where 3D effects exist, for transmittance $T(x)$ for various values of the single scattering albedo ω_0^{cloud} and the solar azimuth ϕ . The solar zenith angle is equal to 60° .

ω_0^{cloud}	$\phi = 180^\circ$		$\phi = 0^\circ$	
	x_r^{aer}	x_r^{cloud}	x_r^{aer}	x_r^{cloud}
0.9	8.75	0.10	0.50	7.75
0.95	8.25	2.30	2.30	8.25
0.99	7.25	4.10	4.50	8.75
1.0	6.75	4.70	4.90	8.75

geneous and semi-infinite along the horizontal coordinates and media have one common vertical plane boundary. All coefficients are calculated using the spatial-angular distribution of radiation intensity obtained by the code RADUGA (Nikolaeva et al., 2005) in the framework of the 2D (x, z) geometry. It is shown how the horizontal “jump” of optical properties leads to the well-known brightening and shadowing effects at the edge of a cloud and in a neighboring clear sky region.

It is shown that these effects are tightly connected with the horizontal radiation transport in broken cloud systems and appear even for nonabsorbing media. The absorption of radiation can enhance or relax these effects in dependence, in particular, on the solar zenith angle.

It should be stressed that we consider only the model problem with the sharp plane vertical interior boundary and not general broken cloud systems. The optical properties of real atmosphere are often changed smoothly and there are intermediate sub-regions with varying concentrations of drops and wet aerosol particles (Redemann et al., 2009). Therefore, the results presented here are only approximately valid for the real-world cloud systems. However, we do hope that they will be found to be useful for better understanding the multi-dimensional radiative transfer in cloudy atmospheres.

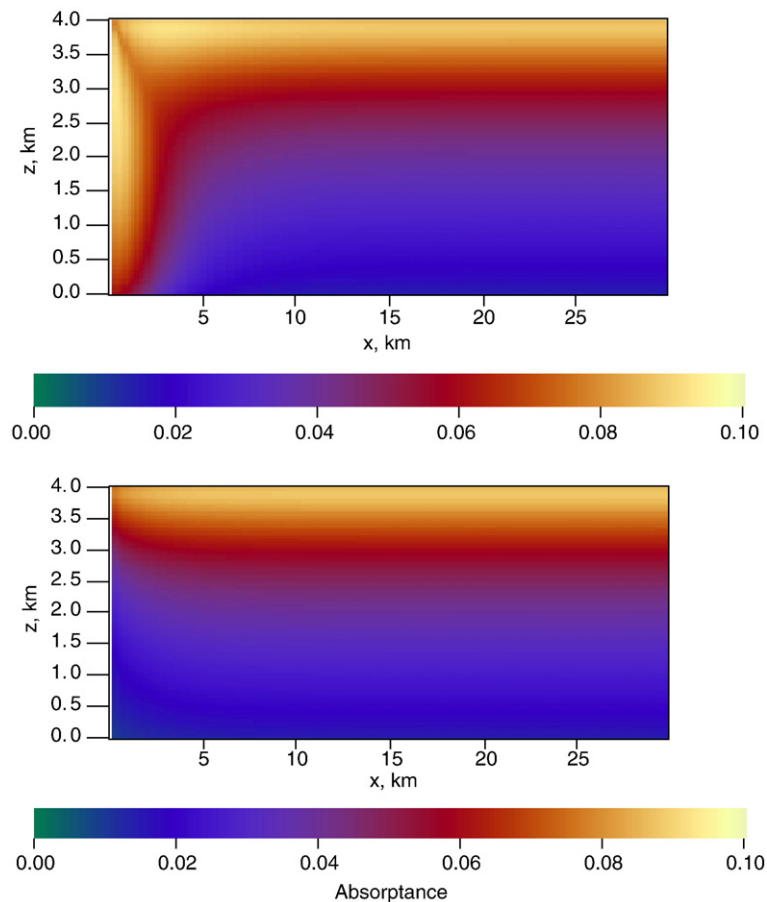


Fig. 6. Absorptance $C(x,z)$ in a cloud at $\omega_0^{cloud} = 0.99$ and illumination from the clear sky side (top) and from the cloud side (bottom). The solar zenith angle is equal to 60° in both cases.

Acknowledgements

This work was supported by the Presidium of Russian Academy of Sciences via research program N14. A. A. Kokhanovsky thanks the German Science Foundation for the support of his research under the Project TERRA (DFG/688/18-1).

References

- Bass, L.P., Germogenova, T.A., Voloschenko, A.V., 1986. Discrete Ordinates Methods in Problems of Radiative Transfer. Keldysh Institute of Applied Mathematics, Moscow.
- Evans, K.F., 1998. The spherical harmonics discrete ordinate method for three-dimensional atmospheric radiative transfer. *Journal of Atmospheric Science* 55, 429–446.
- Larsen, E.W., 1982. Unconditionally stable diffusion-synthetic acceleration methods for the slab geometry discrete-ordinates equations. Part I: theory. *Nuclear Science and Engineering* 82, 47–63.
- Marchuk, G.I., Lebedev, V.I., 1986. Numerical Methods in the Theory of Neutron Transport. OPA, Amsterdam.
- Marshak, A., Knyazikhin, Y., Davis, A.B., Wiscombe, W.J., Pilewskie, P., 2000. Cloud-vegetation interaction: use of normalized cloud index for estimation of cloud optical thickness. *Geophysical Research Letters* 27, 1695–1698.
- Nikolaeva, O.V., Bass, L.P., Germogenova, T.A., Kokhanovsky, A.A., Kuznetsov, V.S., Mayer, B., 2005. The influence of neighboring clouds on the clear sky reflectance studied with the 3-D transport code RADUGA. *Journal of Quantitative Spectroscopy & Radiative Transfer* 94, 405–424.
- Redemann, J., Zhang, Q., Russel, P., Livingston, J., Remer, L., 2009. Case studies of aerosol remote sensing in vicinity of clouds. *Journal of Geophysical Research* 114, D06209.
- Titov, G.A., 1998. Radiative horizontal transport and absorption in stratocumulus clouds. *Journal of Atmospheric Science* 2549–2560.
- van de Hulst, H.C., 1980. Multiple Light Scattering. Academic Press, New York.
- Varnai, T., Marshak, A., 2002. Observations of three-dimensional radiative effects that influence MODIS cloud optical thickness retrievals. *Journal of the Atmospheric Science* 59, 1607–1618.
- Varnai, T., Marshak, A., 2009. MODIS observations of enhanced clear sky reflectance near clouds. *Geophysical Research Letters* 36, L06807.
- Widlowski, J.L., Pinty, B., Lavergne, T., Verstraete, M.M., Gobron, N., 2006. Horizontal radiation transport in 3-D forest canopies at multiple spatial resolutions: simulated impact on canopy absorption. *Remote Sensing of Environment* 103, 379–397.
- Wiscombe, W.J., 1977. The delta-M method: rapid yet accurate radiative flux calculations for strongly asymmetric phase functions. *Journal of the Atmospheric Science* 34, 1408–1422.